CRYSTAL GROWTH & DESIGN

Article

pubs.acs.org/crystal

Crystal Growth, Crystal Structure, Optical Properties, and Phase Transition of $BaCaBO_3F$

Manfred Burianek,[⊥] Michael Teck,[⊥,†] Carolin Niekamp,[⊥] Johannes Birkenstock,[⊥] Iris Spieß,[⊥] Olaf Medenbach,[#] Lennart A. Fischer,[§] Paul E. Wolff,[§] Johannes Neumann,[‡] and Reinhard X. Fischer*[,⊥,∥]

[⊥]Fachbereich Geowissenschaften, Universität Bremen, Klagenfurter Straße, 28359 Bremen, Germany

[#]Institut für Geologie, Mineralogie und Geophysik, Ruhr-Universität Bochum, Bochum, Germany

[§]Institut für Mineralogie, Leibniz Universität Hannover, Callinstrasse 3, 30167 Hannover, Germany

[‡]Fraunhofer Institute for Manufactoring Technology and Advanced Materials, IFAM, Oldenburg, Germany

[∥]MAPEX Center for Materials and Processes, University of Bremen, D-28359, Bremen, Germany

Supporting Information

ABSTRACT: A crystal of $BaCaBO_3F$ was grown by the Czochralski method. It shows a phase transition at 242.7 °C upon cooling where the hexagonal high-temperature modification is transformed to a monoclinic low-temperature form (space group $C2$, a = 17.8779(8) Å, b = 9.0596(4) Å, c = 12.9735(5) Å, β = 118.875(13)°, V = 1840.03(22) Å^3, Z = 18). The monoclinic phase has a symmetry lowered by an index of 18 relative to the hexagonal supergroup. This represents a higher symmetry than the rhombohedral model which has a symmetry of index 36 lower than the hexagonal form determined in a previous study (Li and Zeng, *J. Cryst. Growth* **2013**, *382*, 47). The monoclinic system is confirmed by optical investigations with a polarizing microscope showing biaxial negative character and refractive indices n_x = 1.615(1), n_y = 1.664(1), and n_z = 1.665(1), $2V_x$ = 10.0(2)° as measured on a microrefractometer spindle stage in immersion liquids. Electron microprobe analysis yielded a slight excess of Ba resulting in the composition $Ba_{1.04}Ca_{0.96}BO_3F$ corresponding to $^{[7]}Ba_{4.7}{}^{[8]}Ba_6{}^{[9]}Ba_4{}^{[10]}Ba_4{}^{[7]}Ca_{17.3}{}^{[3]}B_{18}O_{54}F_{18}$ in a crystal-chemical notation for the unit-cell content with the cations in their respective coordination. On the basis of this composition, the mean refractive index <n> can be calculated from individual electronic polarizabilities of the ions resulting in <n_{calc}> = 1.638 which is close to the observed value of <n_{obs}> within an error of 0.5%.

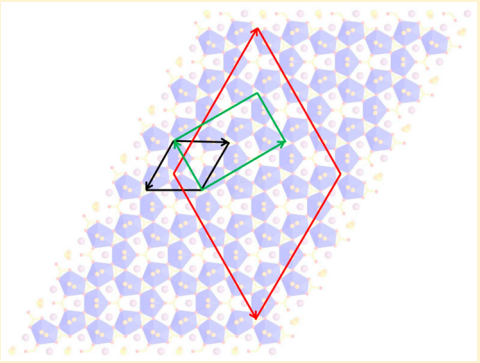

INTRODUCTION

$BaCaBO_3F$ is an interesting material with important nonlinear optical properties. Doped with rare-earth elements it was reported to be a new laser crystal with potential for self-frequency doubling.[1−4] Pure $BaCaBO_3F$ was first obtained by Keszler et al.[5] described as a congruent melting compound crystallizing in the hexagonal space group $P\bar{6}2m$ with a = 9.049(1) Å and c = 4.326(1) Å. Crystals up to several centimeters could be grown by the Czochralski[2,3,6−8] and Kyropoulos[9,10] pulling methods. The basic features of the hexagonal crystal structure were described by Keszler et al. in 1994[5] without publishing the atomic parameters. The crystal structure was derived later by Xu et al.[7] from powder diffraction data by Rietveld refinements, although a melt-grown crystal with a diameter of about 1.5 cm and a length of 2.5 cm was available. The crystal structure determined at room temperature was described in a hexagonal space group with BO_3 groups linking BaO_6F_3 and CaO_5F_2 polyhedra in a disordered fashion with O2 and F on split positions with half occupancies, respectively. The BO_3 groups have an approximately planar arrangement with alternating inclination in the (001) plane due to the disorder of the O2 atoms. Single-crystal studies of $BaCaBO_3F$ to investigate the fluorine vacancies in more detail were proposed but never published. Four years later, Li and Zeng[8] determined a phase transition at 242 °C below which the structure was described in the rhombohedral space group $P3$ with tripled basis vectors in all three directions with respect to the hexagonal supergroup. Above 242 °C the structure was confirmed to be hexagonal essentially representing the model derived by Xu et al.[7] Li and Zeng[8] pointed out that Xu et al.[7] might have missed some superstructure reflections in their powder diffraction pattern and thus have described an average structure analogue to the high-temperature phase, though it was refined against room-temperature data.

$BaCaBO_3F$ came to our attention in the context of our optical studies to determine electronic polarizabilities from refractive indices.[11−13] Specifically, prediction of the refractive indices of borate optical crystals from polarizabilities plays an important role in the search for new linear and nonlinear optical materials.[14] Mean refractive indices can be calculated

Received: April 5, 2016
Revised: June 1, 2016
Published: June 24, 2016

DOI: 10.1021/acs.cgd.6b00518
Cryst. Growth Des. 2016, 16, 4411−4420

from the electronic polarizabilities of the ions using the chemical composition, the molar volume of the formula unit, the coordination numbers from the crystal structure,[12,13] and the Anderson–Eggleton relationship[12,15] relating refractive indices and polarizabilities as briefly explained in the Results. $BaCaBO_3F$ showed an unusual discrepancy between observed and calculated polarizabilities. Consequently, this work was performed to determine if the deviation is caused by a systematic effect or if it is due to an error in either the crystal structure description or the chemical composition or both.

Figure 1. Czochralski grown $BaCaBO_3F$ ($l \approx 40$ mm).

EXPERIMENTAL SECTION

Crystal Growth. $BaCaBO_3F$ is known to melt congruently at about 1100 °C.[7,8] Therefore, the Czochralski method is likely to be the appropriate crystal-growth method for single crystals of this compound grown from a melt of stoichiometric composition. The following chemicals were used for preparation: $BaCO_3$ (Alpha Aesar, 99.95%), $CaCO_3$ (Chempur, 99.9%), H_3BO_3 (Merck, 99.5%), and BaF_2 (Alpha Aesar 99%). The preparation of the starting composition was carried out in two steps. In a first step $BaCa_2(BO_3)_2$ was prepared according to

$$BaCO_3 + 2CaCO_3 + 2H_3BO_3 \rightarrow BaCa_2(BO_3)_2 + 3H_2O + 3CO_2$$

The resulting $BaCa_2(BO_3)_2$ was reacted with BaF_2 in a second step according to

$$BaCa_2(BO_3)_2 + BaF_2 \rightarrow 2BaCaBO_3F$$

In this procedure partial oxidation of BaF_2 at elevated temperature should be avoided.[1]

The mixture was heated below 1000 °C for 24–48 h in a resistance furnace and finally pressed into tablets, which were melted in a platinum crucible with the dimensions Ø 40 × 40 mm^3 suitable for Czochralski growth.

The crystals were grown in an 18 kHz frequency furnace in ambient air with and without an active afterheater for variation of temperature gradients. Seed material was prepared by successively selecting $BaCaBO_3F$ grains from polycrystalline boules grown on a platinum wire as a replacement for a seed crystal. The seed crystals were oriented along [001] in hexagonal setting.

After melt homogenization slightly above the liquidus temperature (1100 °C), the crystals were grown with a pull rate of 0.5 mm/h and a rotation rate of 20 rpm. The crystals were cooled to room temperature at a rate of 10–25 K/h. Several colorless crystals were grown with lengths up to 45 mm and diameters of 10–12 mm (Figure 1).

$BaCaBO_3F$ crystals tend to form cracks near the surface in the lower parts of the boules. In addition, melt alteration occurred during crystal growth. After several growth courses small insoluble particles were observed in the melt. After decanting the melts, an insoluble precipitate of unknown chemical composition was observed on the crucible bottom which clearly indicates melt alteration and shift of melt composition during crystal growth. Therefore, in order to guarantee a homogeneous chemical composition, only one crystal was grown per ingot. The crystals were cut into several pieces for further studies.

Electron Microprobe Analysis (EMPA). One of the Czochralski-grown pieces was analyzed by EMPA using a Cameca SX100 at

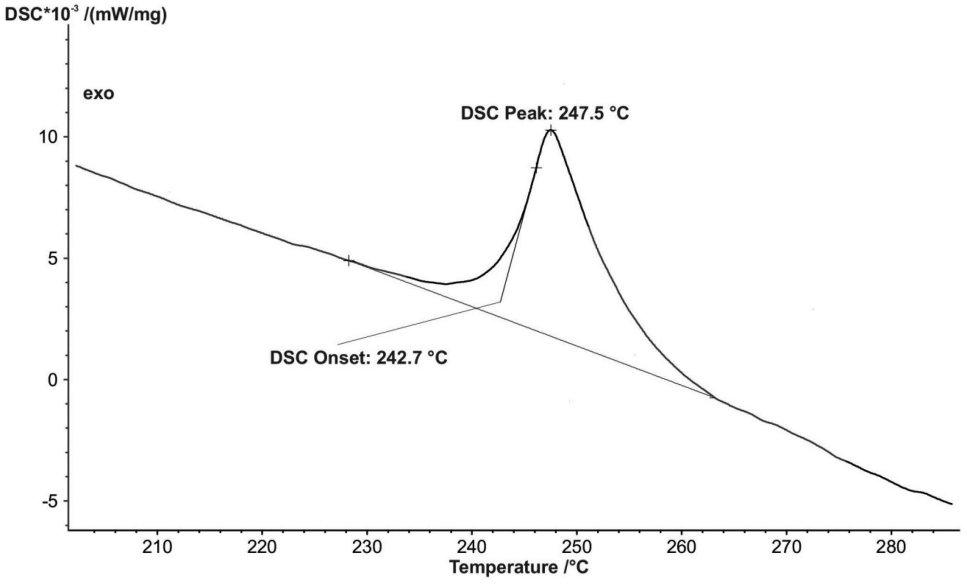

Figure 2. DSC signal showing the endothermic reaction at 242.7 °C corresponding to the phase transition.

DOI: 10.1021/acs.cgd.6b00518
Cryst. Growth Des. 2016, 16, 4411–4420

Table 1. Data Collection Parameters, Refinement Details, and Crystal Data

crystal data	
chemical composition assumed in crystal-structure analysis	$BaCaBO_3F$
space group	$C2$
Z	18
a [Å]	17.8779(8)
b [Å]	9.0596(4)
c [Å]	12.9735(5)
β [°]	118.875(13)
V [Å^3]	1840.03(22)
Data collection and refinement	
temperature [K]	298
no. of measured reflections	102,941
no. of unique reflections	6167
no. $F_0 > 4\sigma(F_0)$	5488
range of h, k, l	$\lvert h\rvert \le 26$, $\lvert k\rvert \le 13$, $-19 \le l \le 18$
θ-max [°]	32.42
no. parameters	287
no. constraints	0
R_{int}/R_σ[a]	0.0602/0.0402
$R_1/R_1 > 4\sigma(F_0)$[a]	0.036/0.025
$wR2$[a]	0.049
GOF[a]	1.007
min Δ [e·Å^{-3}]	−1.13, 0.84 Å from Ba1
max Δ [e·Å^{-3}]	0.96, 0.33 Å from Ba1

[a] Note: $R_{int} = \frac{\sum \lvert F_o^2 - F_o^2(mean)\rvert}{\sum F_o^2}$, $R_\sigma = \frac{\sum \sigma(F_o^2)}{\sum F_o^2}$, $R1 = \frac{\sum \lVert F_o\rvert - \lvert F_c\rVert}{\sum \lvert F_o\rvert}$, $wR2 = \left(\frac{\sum w(F_o^2 - F_c^2)^2}{\sum w(F_o^2)^2}\right)$, $w = \frac{1}{(\sigma(F_o^2))^2 + (0.0278P)^2 + 1.35P}$, $P = \frac{\max(F_o^2, 0) + 2F_c^2}{3}$, GOF $= \sqrt{\frac{\sum w(F_o^2 - F_c^2)^2}{n-p}}$, n = number of reflections, p = total number of parameters refined.

University of Hannover equipped with five spectrometers having a static (fixed) beam. Analyses were carried out using an acceleration voltage of 15 kV and a beam current of 15 nA with a counting time of 10 s for each element on the peak and 5 s on the background. Raw data were corrected with the software "Peak Sight" and PAP matrix correction (Pouchou and Pichoir[16]). Natural minerals wollastonite (Ca), baryte (Ba), and strontiofluorite (F) were used as standards. The results show that the crystal is predominantly homogeneous. However, 50−80 μm inclusions can be observed showing compositional differences to the crystal and between inclusions as well as in a single inclusion. In these inclusions Ba and Ca amounts are increasing with decreasing F and B but always having a Ba/Ca = 1 ratio within the error margins. The elemental analysis yielded 60.44 wt % BaO, 20.47 wt % CaO, and 6.94 wt % F as an average from 18 data points resulting in a molar Ba/Ca/F ratio of 1.04:0.96:0.96 (scaled to a sum of Ba + Ca = 2.0 for better comparison with the chemical formula). Boron was excluded from the analysis because of high uncertainties in its determination. Analyses including B yielded Ba/Ca/B/F = 1.02:0.98:0.36:1.06 with an amount of boron being much too low especially considering that it would cause 15% of oxygen being vacant. Therefore, boron is assumed to represent the stoichiometric complement in this composition yielding $Ba_{1.04}Ca_{0.96}B_{0.99}O_3F_{0.96}$ which closely resembles the ideal composition of $BaCaBO_3F$.[7]

Differential Scanning Calorimetry (DSC). DSC analysis was performed on a STA 449F3 NETZSCH instrument in flowing Ar gas using a heating rate of 5 K/min. It clearly revealed the phase transition already determined by Li and Zeng.[8] The DSC signal (Figure 2) shows an endothermic reaction at an onset temperature of 242.7 °C (peak at 247.5 °C), which agrees well with the temperature of 242 °C reported by Li and Zeng.[8]

Figure 3. Thin section of $BaCaBO_3F$ under the polarizing microscope showing the decomposed fragments with different orientations.

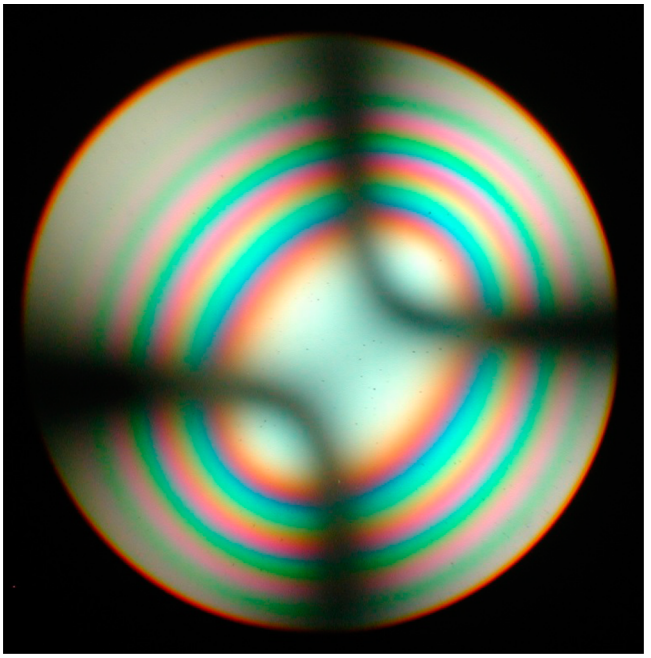

Figure 4. Interference figure of $BaCaBO_3F$ in conoscopic view. Diffraction analysis of another homogeneous fragment of the sample yielded a monoclinic unit cell as shown in Figure 5 for two layers in reciprocal space.

X-ray Powder Diffraction (XRPD). Phase purity was confirmed by XRPD analysis at ambient conditions using a Philips X'Pert diffractometer (Panalytical, Almelo, Netherlands) equipped with an 0.25° divergence slit, an 0.5° anti scatter slit, a soller slit (0.04 rad), and a mask (10 mm wide) in the primary beam, as well as with a soller slit (0.04 rad), a Ni-filter and a X'Celerator detector system (127 channels in 2.122°2θ, i.e., 0.0167°/channel) in the secondary beam using Cu$K\alpha_{1,2}$ radiation. Data were collected from 5 to 120° 2θ, with a step-size of 0.017° and a measuring time of 100 s per step. The same diffractometer equipped with a high-temperature chamber HTK1200N (Anton Paar, Vienna, Austria) was used for data collection up to 900 °C. All data sets were evaluated using the BRASS suite of programs.[17]

Optical Investigations. A polished fraction with homogeneous regions big enough for further optical investigations was studied under the polarizing microscope. One of these fragments, glued to a glass fiber, was mounted on a microrefractometer spindle stage equipped with a second spindle with an internal refractometer (here calcite) to

DOI: 10.1021/acs.cgd.6b00518
Cryst. Growth Des. 2016, 16, 4411−4420

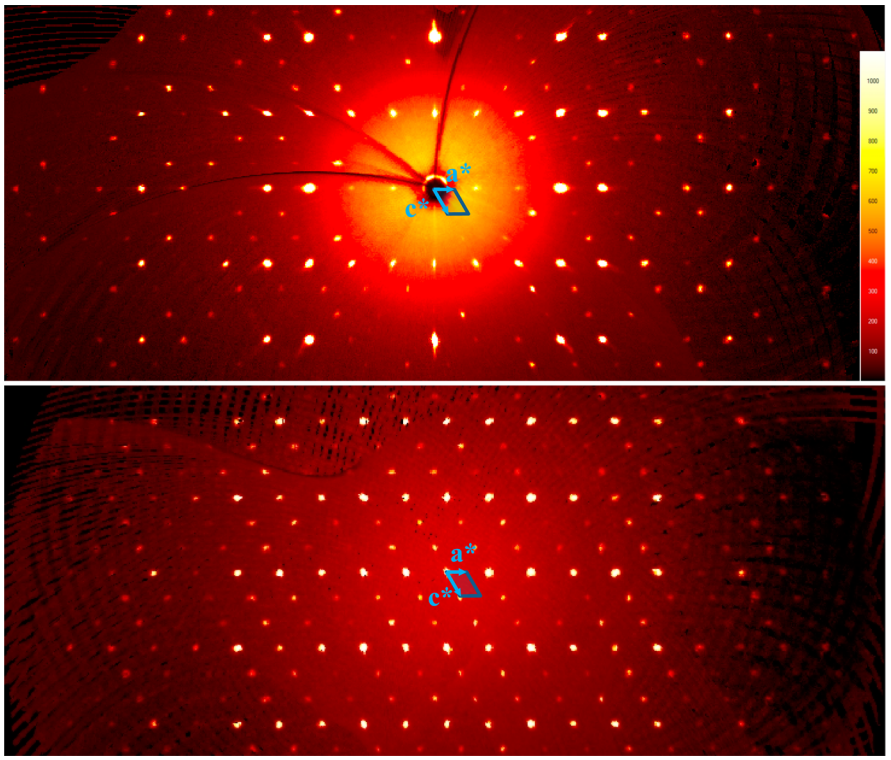

Figure 5. Layer *h*0*l* (top) and *h*4*l* (bottom) of the undistorted reciprocal lattice with the monoclinic reciprocal unit cell projected parallel to **b*** at the origin.

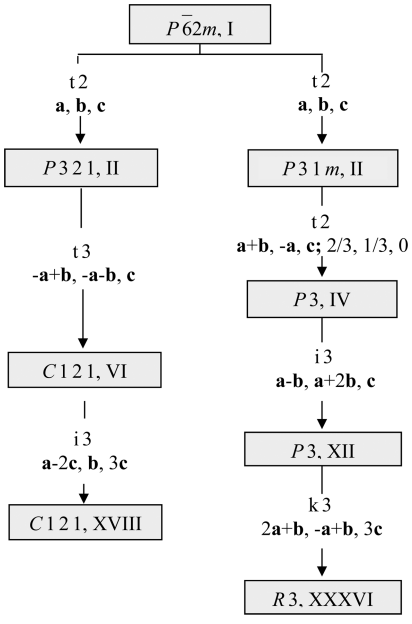

Figure 6. Bärnighausen tree showing the group subgroup relationships. Branches contain information on the type (t = translationengleich, k = klassengleich, i = isomorphic) and the index of symmetry reduction. The symmetry lowering relative to the hexagonal unit cell is indicated by Roman numerals representing the cumulative indices of symmetry reduction following the scheme introduced by Baur and Fischer.[26] An alternative derivation with an orthorhombic symmetry as intermediate step is shown in Figure S1 and Table S3 in the Supporting Information.

determine the indices of refraction of the immersion oil at the moment of its match with the unknown crystal as described by Medenbach.[18] For orienting the crystal the extinction curves[19] were determined by rotating the object spindle in steps of 10° and recording the microscope stage angles for extinction under crossed polarizers. The program EXCALIBRW[20] was used for plotting the extinction curves and to determine the orientation of the axes of the indicatrix.

Single-Crystal X-ray Diffraction (SXD). Another homogeneous fragment of the crystal of approximately 26 × 106 × 138 μm^3 was separated and glued to a glass fiber. Single crystal X-ray diffraction data sets were collected on a Bruker four-circle diffractometer (kappa type) equipped with Mo tube ($\lambda_{K\alpha}$ = 0.71073 Å; 50 kV, 30 mA), Triumph monochromator and Photon100 area detector in a D8 Venture housing. Intensities were recorded by omega scans in steps of 2° for 40 s each. The Bruker Apex2 software (ver. 2014.11-0) was used for data collection, integration, and absorption correction (empirical multiscan method).

Data collection parameters, crystal data, and refinement parameters are listed in Table 1. All refinements were performed with SHELX-97[21,22] within the WINGX[23] user interface and program suite. Crystal-structure projections were drawn with STRUPLO.[24]

RESULTS AND DISCUSSION

The optical investigations under the polarizing microscope immediately revealed that the crystal is decomposed into multiple fragments probably representing twinned lamellae as shown in Figure 3. Surprisingly, the interference figure (obtained in conoscopic configuration of the microscope) of a single domain large enough for optical inspection unambiguously turned out to be biaxial as shown in Figure 4 and to have a negative optical character. The main refractive indices were determined as n_x = 1.615(1), n_y = 1.664(1), and n_z = 1.665(1) with an angle of the acute bisectrix of $2V_x$ = 10.0(2)°, which agrees well with the corresponding value calculated from the refractive indices within the error margins (1.6150, 1.6645, 1.6649 yields $2V_x$ = 10.04°). Thus, it must have a symmetry lower than hexagonal or trigonal.

DOI: 10.1021/acs.cgd.6b00518
Cryst. Growth Des. 2016, 16, 4411−4420

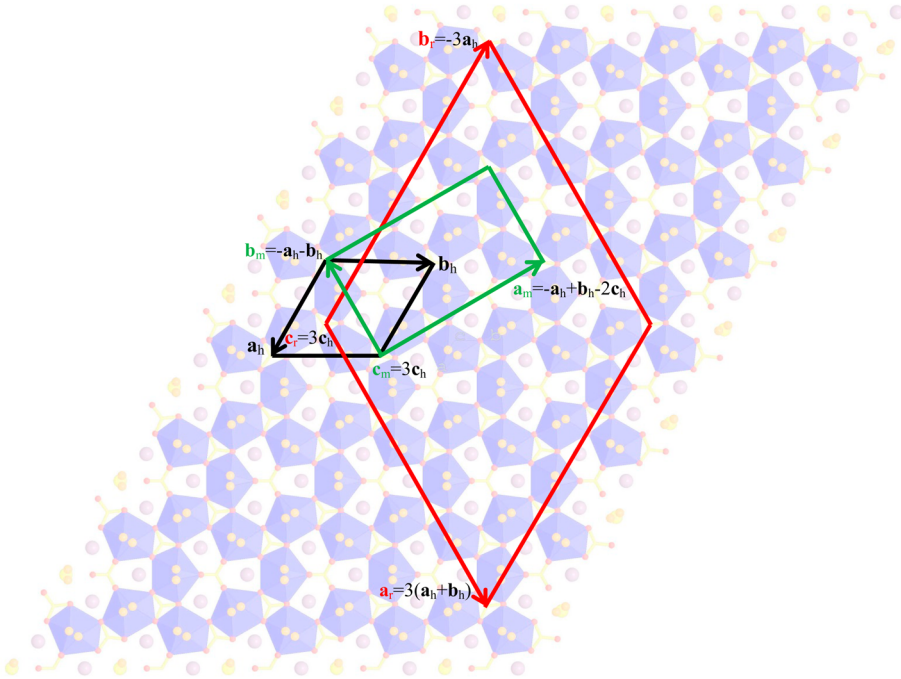

Figure 7. Relationships between hexagonal (h), rhombohedral (r), and monoclinic (m) unit cells projected on top of the hexagonal structure.

Table 2. Atomic Site Relationships of the Monoclinic Branch in Figure 6

$P\bar{6}2m$, I		P 3 2 1, II		C 1 2 1, VI		C 1 2 1, XVIII	
Ba1	[3(g), m 2 m]	Ba1	[3(f), . 2 .]	Ba11	[4(c), 1]	Ba11a	[4(c), 1]
						Ba11b	[4(c), 1]
						Ba11c	[4(c), 1]
				Ba12	[2(b), 2]	Ba12a	[4(c), 1]
						Ba12b	[2(b), 2]
Ca1	[3(f), m 2 m]	Ca1	[3(e), . 2 .]	Ca11	[4(c), 1]	Ca11a	[4(c), 1]
						Ca11b	[4(c), 1]
						Ca11c	[4(c), 1]
				Ca12	[2(a), 2]	Ca12a	[2(a), 2]
						Ca12b	[4(c), 1]
B1	[2(c), $\bar{6}$ . .]	B1	[2(d), 3 . .]	B1	[4(c), 1]	B11	[4(c), 1]
						B12	[4(c), 1]
						B13	[4(c), 1]
B2	[1(a), $P\bar{6}2m$]	B2	[1(a), 3 2 .]	B2	[2(a), 2]	B21	[2(a), 2]
						B22	[4(c), 1]
O1	[6(j), m . .]	O1	[6(g), 1]	O11	[4(c), 1]	O11a	[4(c), 1]
						O11b	[4(c), 1]
						O11c	[4(c), 1]
				O12	[4(c), 1]	O12a	[4(c), 1]
						O12b	[4(c), 1]
						O12c	[4(c), 1]
				O13	[4(c), 1]	O13a	[4(c), 1]
						O13b	[4(c), 1]
						O13c	[4(c), 1]
O2	[6(i), . . m]	O2	[6(g), 1]	O21	[4(c), 1]	O21a	[4(c), 1]
						O21b	[4(c), 1]
						O21c	[4(c), 1]
				O22	[4(c), 1]	O22a	[4(c), 1]
						O22b	[4(c), 1]
						O22c	[4(c), 1]
				O23	[4(c), 1]	O23a	[4(c), 1]
						O23b	[4(c), 1]
						O23c	[4(c), 1]
F1	[6(k), 1]	F1	[6(g), 1]	F11	[4(c), 1]	F11a	[4(c), 1]
						F11b	[4(c), 1]
						F11c	[4(c), 1]
				F12	[4(c), 1]	F12a	[4(c), 1]
						F12b	[4(c), 1]
						F12c	[4(c), 1]
				F13	[4(c), 1]	F13a	[4(c), 1]
						F13b	[4(c), 1]
						F13c	[4(c), 1]

DOI: 10.1021/acs.cgd.6b00518
Cryst. Growth Des. 2016, 16, 4411−4420

Table 3. Atomic Parameters, Equivalent Displacement Parameters, and Wyckoff Positions[a]

atom	atom cif	x	y	z	B_{eq} (Å^2)	Wyckoff position[29]
Ba11a	Ba3	0.86282(2)	0.84563(3)	0.74400(2)	0.99	4(c)
Ba11b	Ba2	0.86108(2)	0.84782(3)	0.07657(2)	0.94	4(c)
Ba11c	Ba1	0.84500(2)	0.86735(2)	0.39691(2)	0.84	4(c)
Ba12a	Ba5	0.00924(2)	0.29371(3)	0.17832(2)	0.91	4(c)
Ba12b	Ba4	0	0.26229(4)	1/2	0.87	2(b)
Ca11a	Ca1	0.69665(6)	0.69512(9)	0.46735(8)	0.63	4(c)
Ca11b	Ca3	0.80629(6)	0.1874(1)	0.20004(8)	0.66	4(c)
Ca11c	Ca2	0.68787(6)	0.68653(9)	0.12480(8)	0.65	4(c)
Ca12a	Ca4	0	0.6032(1)	0	0.61	2(a)
Ca12b	Ca5	0.99897(6)	0.6167(1)	0.33934(8)	0.64	4(c)
B11	B5	0.6650(3)	0.0010(6)	0.4634(5)	0.82	4(c)
B12	B1	0.6658(3)	0.9925(6)	0.0919(5)	0.69	4(c)
B13	B3	0.8321(3)	0.4946(6)	0.2217(5)	0.70	4(c)
B21	B4	0	0.0000(7)	0	0.55	2(a)
B22	B2	−0.0002(3)	−0.0058(6)	0.3343(4)	0.74	4(c)
O11a	O14	0.8473(2)	0.6540(3)	0.5493(3)	1.02	4(c)
O11b	O8	0.6547(2)	0.1434(3)	0.0823(3)	1.16	4(c)
O11c	O3	0.8432(2)	0.6479(3)	0.2283(3)	1.07	4(c)
O12a	O7	0.7473(2)	0.9329(3)	0.1452(3)	1.06	4(c)
O12b	O12	0.7471(2)	0.9452(3)	0.5146(3)	1.08	4(c)
O12c	O13	0.7494(2)	0.4370(3)	0.1619(3)	0.96	4(c)
O13a	O9	0.5953(2)	0.8993(3)	0.0506(3)	1.06	4(c)
O13b	O11	0.5957(2)	0.9071(3)	0.4177(3)	1.04	4(c)
O13c	O10	0.9019(2)	0.4027(3)	0.2726(3)	1.13	4(c)
O21a	O1	0.5625(2)	0.5718(3)	0.0956(3)	1.43	4(c)
O21b	O6	0.5746(2)	0.5677(4)	0.3970(4)	2.45	4(c)
O22b	O5	0.9262(2)	0.0543(4)	0.3249(3)	1.49	4(c)
O23a	O2	0.9981(2)	0.8608(3)	0.2830(3)	2.06	4(c)
O23c	O4	0	0.8478(5)	0	1.16	2(a)
F11a	F3	0.7164(2)	0.6669(3)	0.6476(2)	1.76	4(c)
F11b	F5	0.6485(2)	0.6510(3)	0.9333(2)	1.85	4(c)
F12a	F2	0.6890(2)	0.7344(4)	0.2940(2)	1.87	4(c)
F13a	F4	0.0170(2)	0.5936(3)	0.1810(2)	1.79	4(c)
F13b	F1	0	0.7156(4)	1/2	1.32	2(b)

[a]Atom names are given following the designations in Table 2 with the corresponding names in the cif file in the supporting information. All positions are fully occupied. Note that O23c and F13b are on special positions 2(a) and 2(b), respectively, deviating from the derivation in Table 2.

Table 4. Selected Interatomic Distances [Å]

Ba11a	O23a	2.677(3)	Ba11b	O23a	2.618(3)	Ba11c	O22b	2.676(3)
	O21a	2.762(3)		O11b	2.683(2)		O11a	2.751(2)
	O12b	2.829(3)		O12a	2.697(3)		O12b	2.910(3)
	O12c	2.926(3)		O11c	2.804(2)		O12a	2.926(2)
	O11a	2.966(2)		O12c	2.868(3)		O11c	2.945(2)
	O23c	3.030(1)		O23c	3.088(1)		O21b	2.966(3)
	O11b	3.036(2)		F11b	2.751(3)		F12a	2.723(3)
	O21b	3.259(4)					F13b	2.789(2)
	F11a	2.807(3)					F11a	2.879(3)
	F13a	2.959(3)						
Ba12a	O21a	2.662(3)	Ba12b	O13b × 2	2.747(3)	Ca11a	O21b	2.237(3)
	O13a	2.805(3)		O22b × 2	2.749(3)		O11a	2.399(3)
	O13c	2.902(3)		O21b × 2	2.897(3)		O12b	2.406(3)
	O13b	2.907(2)		O13c × 2	2.898(3)		O12b	2.442(3)
	O13a	2.914(2)					O13b	2.498(3)
	O21b	3.226(4)					F11a	2.205(1)
	F13a	2.720(3)					F12a	2.215(1)
	F11b	2.789(3)						
	F12a	2.866(3)						
Ca11b	O22b	2.307(3)	Ca11c	O21a	2.330(3)	Ca12a	O23c	2.216(5)
	O11b	2.416(3)		O13a	2.417(3)		O13a × 2	2.381(3)
	O12c	2.430(3)		O12a	2.431(3)		O11b × 2	2.464(3)

DOI: 10.1021/acs.cgd.6b00518
Cryst. Growth Des. 2016, 16, 4411−4420

Table 4. continued

	O13c	2.461(3)		O11c	2.457(3)		F13a × 2	2.219(1)
	O12a	2.492(3)		O12c	2.458(3)			
	F11a	2.209(1)		F12a	2.228(1)	B12	O11b	1.378(6)
	F11b	2.2591)		F11b	2.254(1)		O12a	1.385(6)
							O13a	1.392(6)
Ca12b	O23a	2.326(3)	B11	O13b	1.379(6)			
	O11a	2.433(3)		O12b	1.383(6)	B21	O21a × 2	1.368(4)
	O13b	2.435(3)		O11a	1.401(6)		O23c	1.379(8)
	O11c	2.457(3)						
	O13c	2.464(3)	B13	O13c	1.375(6)	B22	O21b	1.357(6)
	F13a	2.238(1)		O12c	1.398(6)		O22b	1.373(6)
	F13b	2.260(2)		O11c	1.400(6)		O23a	1.374(6)

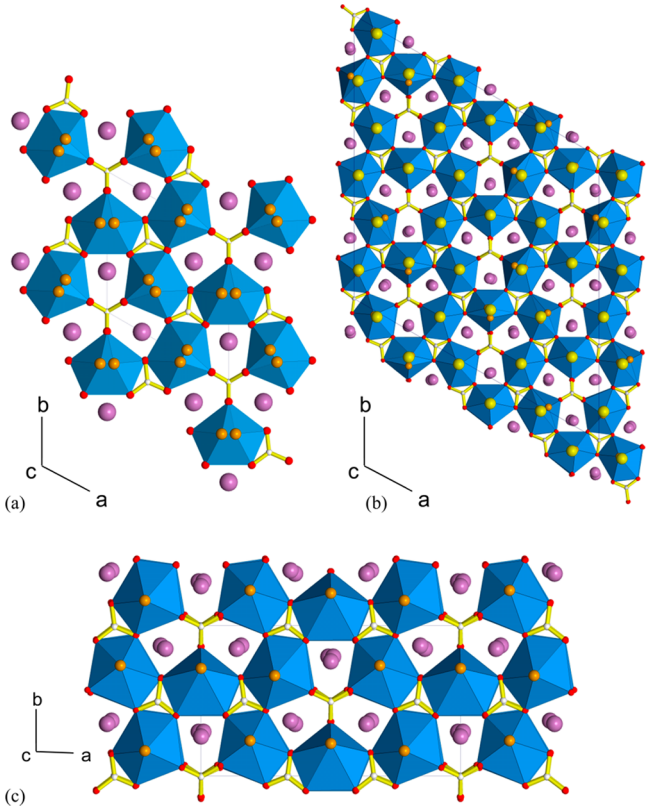

Figure 8. Crystal-structure projections of the (a) hexagonal, (b) rhombohedral, and (c) monoclinic structure with blue CaO_5F_2 polyhedra (O red, F orange), pink Ba atoms, and BO_3 groups.

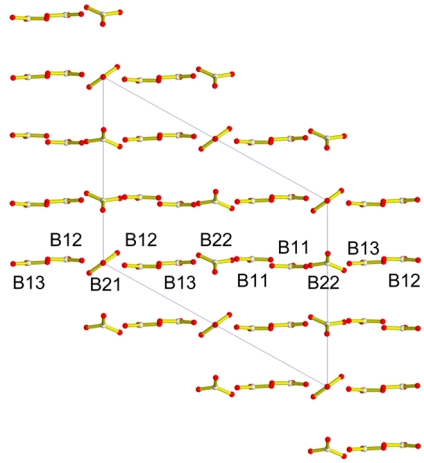

Figure 9. Orientation of BO_3-groups in monoclinic $BaCaBO_3F$. View parallel **−b**.

The transformation from the hexagonal high-temperature modification to the monoclinic low-temperature form corresponds to a symmetry reduction of index 18 relative to the hexagonal supergroup. Consequently, its symmetry is higher than the corresponding rhombohedral structure determined by Li and Zeng,[8] which has a symmetry reduction of index 36. The symmetry relationships are shown in Figure 6 in a Bärnighausen tree[25] with the group subgroup derivations corresponding to the unit-cell relationships shown in Figure 7.

Accordingly, the transformation from the hexagonal unit cell to the rhombohedral unit cell can be expressed as $\mathbf{a}_r = 3(\mathbf{a}_h + \mathbf{b}_h)$, $\mathbf{b}_r = -3\mathbf{a}_h$, $\mathbf{c}_r = 3\mathbf{c}_h$ with an origin shift of 2/3, 1/3, 0. Similarly, the monoclinic unit cell is derived from the hexagonal cell according to $\mathbf{a}_m = -\mathbf{a}_h + \mathbf{b}_h - 2\mathbf{c}_h$, $\mathbf{b}_m = -\mathbf{a}_h - \mathbf{b}_h$, $\mathbf{c}_m = 3\mathbf{c}_h$. Since O2 and F1 are only half occupied in the hexagonal supergroup structure, half of the corresponding sites in the rhombohedral and the monoclinic structures are vacant. These positions are marked in red color in Tables 2 (see also Tables S3 and S4 in the Supporting Information). The assignment of vacant sites is somehow arbitrary in such cases where the corresponding position in the observed structure is close to the center between two split positions. Then the atom with the closer distance was chosen and the other was assumed to be vacant. Two F atoms (F4 and F5) in the rhombohedral structure are on split positions which are mutually exclusive and thus are half occupied. This demonstrates that the rhombohedral model remains disordered even in such a low symmetry. In the monoclinic structure, having a higher symmetry in this special case relative to the trigonal model,[8] all atoms are ordered which is another indication of the preference of the monoclinic symmetry. Final atomic parameters of the monoclinic structure are listed in Table 3, the anisotropic displacement parameters in Table S1, and the deviations between the low-symmetrical structures (rhombohedral and monoclinic) and the hexagonal structure in Table S2 in the Supporting Information. Selected distances and angles are given in Table 4.

The derivation of the monoclinic structure following a path of group-subgroup relations may also explain the above-reported microscopic observation of twinning lamellae as resulting from transformation twinning. As the symmetry group of the lattice changes and as the volume of the unit cell increases significantly we expect to observe twinning by reticular (pseudo-) merohedry.[27,28] This general idea is also supported by the close relationship between the high- and the low-temperature structure as documented in Table 2.

The basic principles of the hexagonal high-temperature structure are essentially retained in the monoclinic low-temperature

DOI: 10.1021/acs.cgd.6b00518
Cryst. Growth Des. 2016, 16, 4411−4420

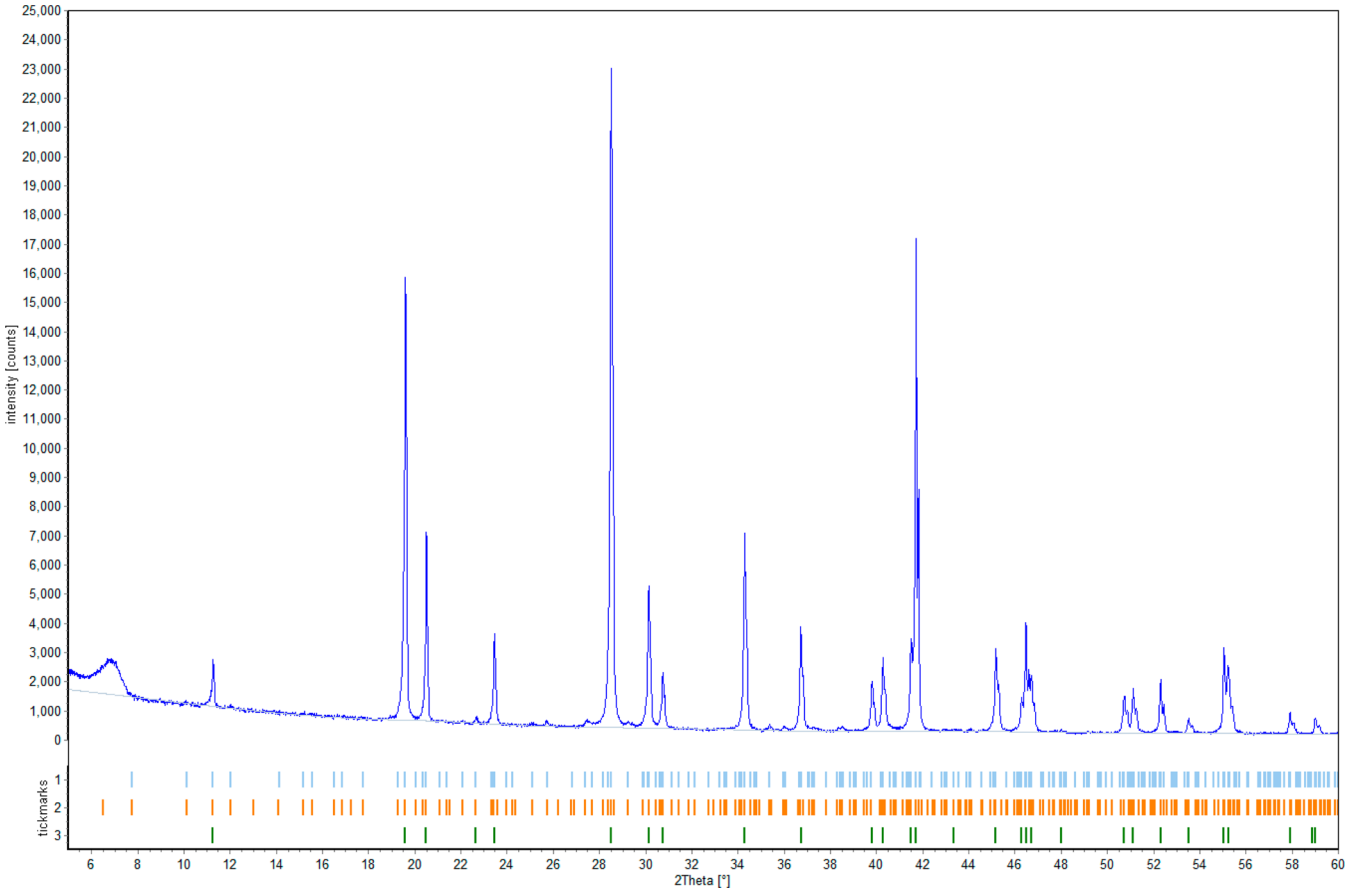

Figure 10. Powder patterns of $BaCaBO_3F$ at room temperature. Tickmarks indicate peak positions (monoclinic mon, trigonal tri, hexagonal hex). The broad hump between 6 and 8° 2θ is an instrumental effect.

modification of $BaCaBO_3F$ as shown in Figure 8. Ca is coordinated by five O and two F atoms forming a pentagonal bipyramid with the O atoms in the central plane and the F atoms forming the apexes on either side. These CaO_5F_2 groups build up a three-dimensional network by corner sharing with two types of BO_3 groups cross-linking the bipyramids perpendicular to [001] in the $(20\bar{3})$ plane (which corresponds to the (001) plane in hexagonal symmetry). The Ba atoms reside in the small channels parallel [001] formed by 3 Ca polyhedra and a BO_3 group as shown in Figure 8. The lowering of the symmetry from the hexagonal to the monoclinic system is mainly caused by the ordering scheme of the BO_3 units being disordered in the hexagonal unit cell and fully ordered in the monoclinic structure as shown in Figure 9. While the BO_3 groups derived from B1 in the hexagonal supergroup are aligned in the $(20\bar{3})$ plane, the BO_3 groups derived from B2 are inclined to this plane following one of the two possible orientations in the hexagonal structure.

Upon heating, $BaCaBO_3F$ undergoes a phase transition as observed by Li and Zeng[8] and shown in Figure 2 in the Experimental Section. This means that a phase transition from hexagonal to monoclinic occurs when the crystal grown in the Czochralski process (Figure 1) is cooled to room temperature. Figure 10 shows the powder patterns of $BaCaBO_3F$ recorded in a heating chamber at ambient temperatures. Tickmarks indicate the peak positions calculated from the three crystal-structure models (monoclinic, trigonal, hexagonal) showing that the main reflections are retained from the hexagonal substructure, while it is difficult to distinguish between the peak positions of the monoclinic and trigonal superstructures. The thermal expansion of the unit-cell volume up to 900 °C is approximately linear as shown in Figure 11.

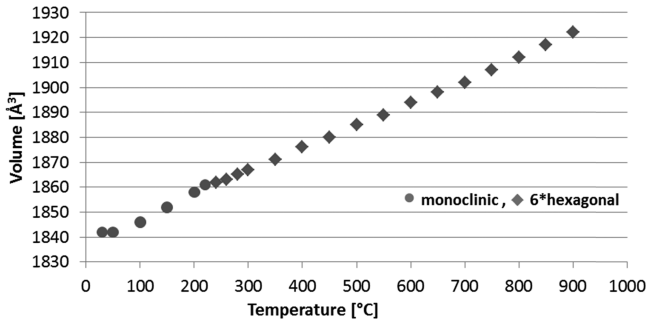

Figure 11. Unit-cell volumes plotted versus temperature. The volume of the hexagonal unit cell is multiplied by 6 to conform to the range of the monoclinic structure.

Recalling that the aim of this work was primarily the clarification of the discrepancy in the optical properties of $BaCaBO_3F$, the deviation between calculated and observed refractive indices >5% can now be explained entirely by the structural differences between the structure as described by the authors[7] and as analyzed here. Mean refractive indices (RI) can be calculated using the additivity rule for electronic polarizabilities of elements as explained by Shannon and Fischer[12] if the chemical composition, the valencies, the coordination numbers of the cations, and the molar volume are known; i.e., the RI of

DOI: 10.1021/acs.cgd.6b00518
Cryst. Growth Des. 2016, 16, 4411−4420

Table 5. Calculated and Observed Refractive Indices and Electronic Polarizabilities for the Hexagonal,[7] Trigonal,[8] and Monoclinic (This Work) Model Calculated on Basis of One Formula Unit of $BaCaBO_3F$[a]

space group	n_e/n_x	n_o/n_y	n_z	$<n_{obs}>$	n_{calc}	Δn [%][g]	α_{obs} [Å^3]	α_{calc} [Å^3]	$\Delta\alpha$ [%]
$P-62m$[b]	1.6145	1.6638		1.6474[7]	1.6171	1.8	11.041	10.531	4.6
$P-62m$[b]	1.6150	1.6647		1.6481[10]	1.6171	1.9	11.054	10.531	4.7
$P-62m$[c]	1.6145	1.6638		1.6474[7]	1.6361	0.7	11.041	10.851	1.7
$P-62m$[c]	1.6150	1.6647		1.6481[10]	1.6361	0.7	11.054	10.851	1.8
$R3$[d]				1.6478[h]	1.6299	1.1	11.059	10.754	2.8
$C2$[e]	1.615(1)	1.664(1)	1.665(1)	1.648	1.634	0.9	11.049	10.809	2.2
$C2$[f]	1.615(1)	1.664(1)	1.665(1)	1.648	1.638	0.6	11.049	10.882	1.5

[a]Chemical compositions are scaled to one formula unit of $BaCaBO_3F$ for the calculation of the polarizabilities. Footnote b refers to 11-coordinated Ba as listed in Table 3 in Xu et al.,[7] footnote c refers to 8-coordinated Ba considering that O2 is only half occupied and the cutoff for including anions in the coordination is after the 8th atom. [b]$^{[11]}Ba^{[7]}Ca^{[3]}BO_3F$. [c]$^{[8]}Ba^{[7]}Ca^{[3]}BO_3F$. [d]$(^{[8]}Ba_{27}{}^{[9]}Ba_{36}{}^{[10]}Ba_{18}{}^{[7]}Ca_{81}{}^{[3]}B_{81}O_{243}F_{81})/81$. [e]$(^{[7]}Ba_4{}^{[8]}Ba_6{}^{[9]}Ba_4{}^{[10]}Ba_4{}^{[7]}Ca_{18}{}^{[3]}B_{18}O_{54}F_{18})/18$ (stoichiometric $BaCaBO_3F$). [f]$(^{[7]}Ba_{4.7}{}^{[8]}Ba_6{}^{[9]}Ba_4{}^{[10]}Ba_4{}^{[7]}Ca_{17.3}{}^{[3]}B_{18}O_{54}F_{18})/18$ (Ba/Ca ratio from EMPA). [g]The deviation delta (Δ) between observed and calculated values is defined as (obs-calc)/obs. [h]Mean value from two references[7,10] in lack of data for the trigonal compound.

hexagonal $BaCaBO_3F$ with Ba 11-coordinated (following the listing of interatomic distances in Table 3 of Xu et al.[7]) can be calculated as follows: The chemical composition can be given as $^{[11]}Ba^{[7]}Ca^{[3]}BO_3F$ in a crystal-chemical notation with coordination numbers (CN) in square brackets. The total electronic polarizability α of $BaCaBO_3F$ thus is obtained by adding the individual contributions of cations and anions according to $\alpha(^{[11]}Ba)+\alpha(^{[7]}Ca)+\alpha(^{[3]}B)+3\cdot\alpha(O)+\alpha(F)$ where the polarizabilities of the cations are taken from Shannon and Fischer[12] and the polarizabilities of the anions are calculated according to $\alpha_- = \alpha_-^o \cdot 10^{-N_o/V_{an}^{1.20}}$ with α_- representing the anion polarizability, V the molar volume of the anions, and α_-^o and N_0 being parameters listed in Shannon and Fischer.[12] This yields a total calculated polarizability α = 10.53 Å^3 for hexagonal $BaCaBO_3F$. This value can be compared with α = 11.04 Å^3 or α = 11.05 Å^3 derived from the observed RI's taken from Xu et al.[7] and Wang et al.[10] using the Anderson–Eggleton relationship[12,15] $\alpha = \frac{(n^2-1)V_m}{4\pi + \left(\frac{4\pi}{3} - 2.26\right)(n^2-1)}$ with the molar volume V_m and the refractive index n corresponding to a deviation of 4.6% and 4.7%, respectively, between observed and calculated values.

However, a careful evaluation of structural details reveals that the CN of Ba in hexagonal $BaCaBO_3F$ can be better described in an 8-coordination. It must be considered that O2 is on a split position being only half occupied, and thus only half of the O2 atoms are involved in the bonds to Ba. Similarly F is not on the 3-fold Wyckoff position[29] 3g as stated in Table 2 in Xu et al.[7] but instead it is on 6k. On the basis of these corrections, the deviation between observed and calculated polarizabilities is reduced to 1.7% and 1.8%, respectively.

Similar calculations yield deviations of 2.8% for the rhombohedral structure.[8] The monoclinic model derived here yields a deviation of 2.2% based on a stoichiometric composition of $BaCaBO_3F$ ($^{[7]}Ba_4{}^{[8]}Ba_6{}^{[9]}Ba_4{}^{[10]}Ba_4{}^{[7]}Ca_{18}{}^{[3]}B_{18}O_{54}F_{18}$). Considering that the EMPA results indicate a chemical composition with slightly higher Ba content and assuming that some of the Ca is replaced by Ba resulting in the formula $^{[7]}Ba_{4.7}{}^{[8]}Ba_6{}^{[9]}Ba_4{}^{[10]}Ba_4{}^{[7]}Ca_{17.3}{}^{[3]}B_{18}O_{54}F_{18}$ the corresponding deviation is 1.5% as shown in Table 5 in comparison with the hexagonal and rhombohedral models.

These results demonstrate that obvious errors in the symmetry of $BaCaBO_3F$ at room temperature do not significantly affect the prediction of refractive indices from the chemical composition yielding RI's with errors close to 1% for all three crystal systems. However, the smallest error of 0.6% is obtained for the monoclinic phase.

$BaCaBO_3F$ is closely related to hexagonal $BaZnBO_3F$ (space group $P\bar{6}$) with ZnO_3F_2 trigonal bipyramids and monoclinic $BaMgBO_3F$ (space group Cc) with MgO_4F_2 octahedra,[30] while $BaCaBO_3F$ contains the pentagonal CaO_5F_2 bipyramids.

CONCLUSIONS

Czochralski-grown crystals of $BaCaBO_3F$ undergo a phase transition from hexagonal to lower symmetry upon cooling to room temperature as described by Li and Zeng[8] and confirmed in this work. However, we found that the low-temperature phase is monoclinic with a symmetry lowering of index 18 relative to the hexagonal structure in contrast to the description by Li and Zeng who determined a rhombohedral structure with an index 36 lower in symmetry. Thus, the monoclinic model presented here has a higher symmetry by an index of 2 compared with the rhombohedral structure. We suspect that the phase transition causes a twinning of the crystal about the **c** axis presumably resulting in triplet domains oriented in such a way that they seem to have a rhombohedral symmetry with all three axes tripled with respect to the hexagonal supergroup. A reinterpretation of the coordination behavior of Ba in the hexagonal structure revealed that the observed refractive indices are consistent with indices calculated from the chemical composition following the procedure described by Shannon and Fischer.[12]

ASSOCIATED CONTENT

Supporting Information

The Supporting Information is available free of charge on the ACS Publications website at DOI: 10.1021/acs.cgd.6b00518.

Anisotropic displacement parameters, table with deviations from hexagonal symmetry, alternative derivation of atomic site relationships, atomic site relationships of the rhombohedral branch (PDF)

Accession Codes

CCDC 1472307 contains the supplementary crystallographic data for this paper. These data can be obtained free of charge via www.ccdc.cam.ac.uk/data_request/cif, or by emailing data_request@ccdc.cam.ac.uk, or by contacting The Cambridge Crystallographic Data Centre, 12 Union Road, Cambridge CB2 1EZ, UK; fax: +44 1223 336033.

DOI: 10.1021/acs.cgd.6b00518
Cryst. Growth Des. 2016, 16, 4411–4420

AUTHOR INFORMATION

Corresponding Author

*E-mail rfischer@uni-bremen.de.

Present Address

†Chemische Kristallographie fester Stoffe, Institut für Anorganische Chemie, Universität Bremen, 28359 Bremen, Germany.

Funding

This project was funded by the Deutsche Forschungsgemeinschaft under Grant Fi442/21-1.

Notes

The authors declare no competing financial interest.

ACKNOWLEDGMENTS

We thank Robert D. Shannon (Boulder, USA) for his comments on the manuscript and his valuable contribution to this work as well as an anonymous reviewer for the comments on the symmetry derivations.

ABBREVIATIONS

CN, coordination number; DSC, differential scanning calorimetry; EMPA, electron microprobe analysis; RI, refractive index; SXD, single-crystal X-ray diffraction; XRPD, X-ray powder diffraction

REFERENCES

(1) Schaffers, K. I.; DeLoach, L. D.; Payne, S. A. Crystal growth, frequency doubling, and infrared laser performance of Yb^{3+}:$BaCaBO_3F$. *IEEE J. Quantum Electron.* **1996**, *32*, 741−748.

(2) Zhao, W.; Zhou, W.; Song, M.; Wang, G.; Du, J.; Yu, H.; Chen, J. Crystal growth and Judd-Ofelt analysis of novel Tm^{3+}-doped $BaCaBO_3F$ crystal. *Optoelectron. Adv. Mater., Rapid Commun.* **2011**, *5*, 49−53.

(3) Zhao, W.; Zhou, W.; Song, M.; Wang, G.; Du, J.; Yu, H.; Chen, J. Polarized spectroscopic properties of a potential self-frequency doubling crystal, Nd^{3+}:$BaCaBO_3F$. *Opt. Mater.* **2011**, *33*, 647−654.

(4) Lin, H.; Zhang, G.; Tanner, P. A.; Liang, H. VUV-Vis Luminescent Properties of $BaCaBO_3F$ Doped with Ce^{3+} and Tb^{3+}. *J. Phys. Chem. C* **2013**, *117*, 12769−12777.

(5) Keszler, D. A.; Akella, A.; Schaffers, K. I.; Alekel, T. New borate structures for NLO applications. In *New Materials for Advanced Solid State Lasers*; Chai, B. H. T., Payne, S. A., Fan, T. Y., Cassanho, A., Allik, T. H., Eds. Materials Research Society, 1994; Vol. *329*, pp 15−22.

(6) Lebedev, V. A.; Voroshilov, I. V.; Ignatiev, B. V.; Gavrilenko, A. N.; Pisarenko, V. F.; Saakyan, A. V. Spectroscopic properties of $CaBaBO_3F$ (CBFB) and $Ca_4Y(BO_3)_3O$ (YCOB) crystals with Yb^{3+} and Er^{3+} ions. In *Advanced Solid State Lasers, Proceedings*; Injeyan, H.; Keller, U.; Marshall, C., Eds., Optical Society of America, Washington, DC., 2000; Vol. *34*, pp 572−574.

(7) Xu, K.; Loiseau, P.; Aka, G. $BaCaBO_3F$: A nonlinear optical crystal investigated for UV light generation. *J. Cryst. Growth* **2009**, *311*, 2508−2512.

(8) Li, R. K.; Zeng, Q. D. Crystal growth, structure and phase transition of the nonlinear optical crystal $BaCaBO_3F$. *J. Cryst. Growth* **2013**, *382*, 47−51.

(9) Zhang, G. C.; Liu, H. J.; Wang, X.; Fan, F. D.; Fu, P. Z. Growth and characterization of nonlinear optical crystal $BaCaBO_3F$. *J. Cryst. Growth* **2006**, *289*, 188−191.

(10) Wang, X.; Zhang, G.; Zhao, Y.; Fan, F.; Liu, H.; Fu, P. Optical properties of $BaCaBO_3F$ crystal. *Opt. Mater.* **2007**, *29*, 1658−1661.

(11) Shannon, R. D.; Shannon, R. C.; Medenbach, O.; Fischer, R. X. Refractive index and dispersion of fluorides and oxides. *J. Phys. Chem. Ref. Data* **2002**, *31*, 931−970.

(12) Shannon, R. D.; Fischer, R. X. Empirical electronic polarizabilities of ions for the interpretation of refractive indices. I. oxides and oxysalts. *Am. Mineral.* **2016**, in press. DOI: 10.2138/am-2016-5730.

(13) Shannon, R. D.; Fischer, R. X. Empirical electronic polarizabilities in oxides, hydroxides, oxyfluorides, and oxychlorides. *Phys. Rev. B* **2006**, *73* (235111), 1−27.

(14) Qin, F.; Li, R. K. Predicting refractive indices of the borate optical crystals. *J. Cryst. Growth* **2011**, *318*, 642−644.

(15) Eggleton, R. A. Gladstone-Dale constants for the major elements in silicates: Coordination number, polarizability, and the Lorentz-Lorentz relation. *Can. Mineral.* **1991**, *29*, 525−532.

(16) Pouchou, J. L.; Pichoir, F. Quantitative analysis of homogeneous or stratified microvolumes applying the model "PAP". In *Electron Probe Quantitation*; Heinrich, K. F. J.; Newbury, D. E., Eds., 1991; pp 31−75.

(17) Birkenstock, J.; Fischer, R. X.; Messner, T. *BRASS*, the Bremen Rietveld Analysis and Structure Suite, Version 2.0.1. www.brass.uni-bremen.de.

(18) Medenbach, O. A new microrefractometer spindle-stage and its application. *Fortschr. Mineral.* **1985**, *63*, 111−133.

(19) Bloss, F. D. *The Spindle Stage: Principles and Practice*; Cambridge University Press: Cambridge, 1981.

(20) Gunter, M. E.; Bandli, B. R.; Bloss, F. D.; Evans, S. H.; Su, S. C.; Weaver, R. Results from a McCrone spindle stage short course, a new version of EXCALIBRW, and how to build a spindle stage. *Microscope* **2004**, *52*, 23−39.

(21) Sheldrick, G. M. *SHELXL-97, a Program for Crystal Structure Refinement*, Release 97-2; University of Göttingen: Göttingen1997.

(22) Sheldrick, G. M. A short history of SHELX. *Acta Crystallogr., Sect. A: Found. Crystallogr.* **2008**, *64*, 112−122.

(23) Farrugia, L. J. WinGX suite for small-molecule single-crystal crystallography. *J. Appl. Crystallogr.* **1999**, *32*, 837−838.

(24) Fischer, R. X.; Messner, T. *STRUPLO*, a new version of the structure drawing program, www.brass.uni-bremen.de.

(25) Bärnighausen, H. *Match* **1980**, *9*, 209−233.

(26) Baur, W. H.; Fischer, R. X. *Zeolite-Type Crystal Structures and Their Chemistry. Zeolite Structure Codes ABW to CZP*. Subvolume B in Landolt-Börnstein, Numerical data and functional relationships in science and technology, New Series, Group IV: Physical Chemistry, Vol. 14, Microporous and other framework materials with zeolite-type structures. Baur, W.H., Fischer, R.X., Eds.; Springer-Verlag: Berlin, 2000.

(27) Nespolo, M.; Ferraris, G. Geminography − The science of twinning applied to the early-stage derivation of non-merohedric twin laws. *Z. Kristallogr. - Cryst. Mater.* **2003**, *218*, 178−181.

(28) Nespolo, M.; Ferraris, G. Applied geminography − symmetry analysis of twinned crystals and definition of twinning by reticular polyholohedry. *Acta Crystallogr., Sect. A: Found. Crystallogr.* **2004**, *60*, 89−95.

(29) Hahn, T. *International Tables for Crystallography*; Springer: Berlin, 2005.

(30) Li, R. K.; Chen, P. Cation coordination control of anionic group alignment to maximize SHG effects in the $BaMBO_3F$ (M = Zn, Mg) series. *Inorg. Chem.* **2010**, *49*, 1561−1565.

DOI: 10.1021/acs.cgd.6b00518
Cryst. Growth Des. 2016, 16, 4411−4420